Int. J. Heat Mass Transfer. Vol. 33, No. 1, pp. 19–27, 1990
Printed in Great Britain

0017–9310/90 $3.00 + 0.00

Unsteady mixed convection about a porous rotating sphere

P. HATZIKONSTANTINOU
Department of Engineering Science, Division of Applied Mathematics and Mechanics, University of Patras, GR 26110 Patras, Greece

(*Received* 23 *August* 1988 *and in final form* 13 *April* 1989)

Abstract—This paper presents the study of the flow and heat transfer characteristics in unsteady boundary layer growth over a rotating sphere in forced flow caused by a uniformly accelerated free stream velocity. Results are presented for gases with a Prandtl number of 0.71 and various buoyancy and rotational values when the surface is solid or porous subjected to suction or injection. A numerical method is applied for which the conditions for stability and optimal convergence are determined. It is found that the local Nusselt number and the local friction factor increase with increasing buoyancy for aiding flow and suction while they decrease with increasing buoyancy and injection. The threshold of significance of buoyancy forces decreases as injection increases and increases as suction increases.

INTRODUCTION

THE ROLE of the buoyancy force on the forced and free convection heat transfer about the axisymmetric round-nosed bodies for the cases of aiding and opposing flows has been studied in the steady state by several authors [1–3]. The neglect of the buoyancy force, which is due to the density variation when the temperature difference between the surface and the fluid is large, may not be justified when the velocity is small. The determination of the thermal boundary layer properties in the case of mixed convection are of particular interest because of their practical implications.

The problem of mixed forced and free convection about a non-rotating sphere has been studied by Chen and Mucoglu [4] while the effect of the mixed flow in a laminar boundary layer over a rotating sphere has been investigated by Rajasekaran and Palekar [5]. In both cases appropriate coordinate transformations are used so that the partial differential equations of the problem are reduced to equations involving derivatives with respect to only one variable. The equations obtained are solved numerically under various velocity and thermal boundary conditions. In the case of very small Reynolds and Grashof numbers analytical solutions have been presented on the problem of mixed forced and free convection about a sphere by Hieber and Gebhart [6]. Under the same conditions experimental results have been reported by Yuge and Klyachko [7, 8].

Although unsteady hydrodynamic flow with or without heat transfer has been studied extensively in the cases of infinite plates [9] it seems that very little work has been carried out on unsteady axial flow past a body of revolution like a sphere or a cylinder [10].

The problem to be tackled here is the unsteady flow of a viscous incompressible fluid around the surface of a rotating sphere. The effect of the buoyancy force on the flow arising from the combination of rotation and forced flow is studied at large Reynolds and Grashof numbers. The analysis is carried out for both aiding and opposing flows in which the buoyancy force aids and opposes the forced convective flow, respectively. The boundary layer growth on a spinning sphere is studied for an impermeable and a porous surface, respectively. In the second case the sphere is subjected to suction or injection of fluid of the same kind. Results are presented for gases having a Prandtl number of 0.71 and for two constant values of the angular velocity ω. A numerical technique based on the finite difference approximation using the explicit method [11] has been developed for our case where several variables are involved and the criteria for stability and convergence are determined.

ANALYSIS AND SOLUTION METHOD

Consider an unsteady incompressible flow about a rotating sphere of radius r_0 which is placed in a flow field with free stream potential velocity $U' = 1.5U_0 \sin(x'/r_0) f(t')$ and a constant temperature T'_∞. U_0 is a constant velocity and $f(t')$ a dimensionless function of time t'. The rotational axis of the sphere is parallel to the free stream velocity and opposite to the gravitational field as shown in the inset of Fig. 1. The fluid properties are constant except that the density changes produce buoyancy forces. We consider a curvilinear coordinate system (x', y', φ') such that x' is measured along a meridian from the first stagnation point and y' measures the distance normal to the surface. The radial distance from a surface element to the axis of symmetry is denoted $r'(x') = r_0 \sin(x'/r_0)$.

If u', v', w' are the components of the velocity field and T' the temperature, the equations which govern the boundary layer are given by

NOMENCLATURE

a, a_i coefficients of the partial derivatives
C_f local friction factor
c constant vertical velocity at the surface
C_+, C_0, C_- injection, solid wall and suction, respectively
g dimensionless gravitational acceleration
h_c local heat transfer coefficient
h step of space variables
Gr Grashof number, $g\beta(T_w - T_\infty)r_0^3/v^2$
K thermal conductivity
k step of time variable
L function of the second-order numerical approximations
Nu local Nusselt number, hr_0/K
Nu_0 local Nusselt number at the stagnation point
Pr Prandtl number, v/a
q_w local surface heat transfer rate per unit area
r_0 radius of sphere
r_s ratio, k/h^2
r radial distance from symmetrical axis to surface
Re Reynolds number, $U_0 r_0/v$
t time
T fluid temperature
T_w wall temperature
T_∞ free stream temperature
U local free stream velocity
U_0 undisturbed oncoming free stream velocity
U_e time independent local free stream velocity
u velocity component in the x-direction
u^* velocity ratio, u/U
v velocity component in the y-direction
w velocity component in the direction of rotation
w^* velocity ratio, w/ω
x coordinate measured along the surface from the stagnation point
y coordinate measured normal to x
z coordinate measured in the direction of rotation.

Greek symbols

α thermal diffusivity
β thermal expansion coefficient
δ_u velocity boundary layer thickness
δ_θ thermal boundary layer thickness
θ dimensionless temperature
θ_0 Heaviside step function
Λ buoyancy parameter, Gr/Re^2
ν_0 kinematic viscosity
τ local wall stress, $0.5C_f Re^{1/2}$
ω_s, ω_l small and large angular velocity, respectively.

Superscript

$'$ dimensional quantities.

$$\frac{\partial}{\partial x'}(r'u') + \frac{\partial}{\partial y'}(r'v') = 0 \tag{1}$$

$$\frac{\partial u'}{\partial t'} + u'\frac{\partial u'}{\partial x'} + v'\frac{\partial u'}{\partial y'} - \frac{w'^2}{r'}\frac{\partial r'}{\partial x'} = \frac{dU'}{dt'} + \nu_0\frac{\partial^2 u'}{\partial y'^2} \pm g\beta(T' - T'_\infty)\sin(x'/r_0) \tag{2}$$

$$\frac{\partial w'}{\partial t'} + u'\frac{\partial w'}{\partial x'} + v'\frac{\partial w'}{\partial y'} + \frac{w'u'}{r'}\frac{\partial r'}{\partial x'} = \nu_0\frac{\partial^2 w'}{\partial y'^2} \tag{3}$$

$$\frac{\partial T'}{\partial t'} + u'\frac{\partial T'}{\partial x'} + v'\frac{\partial T'}{\partial y'} = \frac{\nu_0}{Pr}\frac{\partial^2 T'}{\partial y'^2} \tag{4}$$

subjected to the boundary conditions

$$u' = v' = w' = T' = 0 \quad \text{at} \quad t' \leqslant 0$$

$$u' = 0, \quad v' = c', \quad w' = r'(x')\omega', \quad T' = T'_w \quad \text{at} \quad y' = 0, \quad t' > 0$$

$$u' = U', \quad w' = 0, \quad T' = T'_\infty \quad \text{at} \quad y' \to \infty, \quad t' > 0. \tag{5}$$

Let us consider that T'_w represents the uniform temperature of the surface of the sphere. Then in equation (2) the positive and negative signs are to be taken for aiding ($T'_w < T'_\infty$) and opposing ($T'_w > T'_\infty$) flows, respectively. The radial velocity of the fluid $v' = c'$ is considered to be a constant at the surface. For an impermeable surface we have $c' = 0$ while in the case of a porous surface fluid is sucked ($c' < 0$) or injected ($c' > 0$) with a constant value.

The following non-dimensional variables and parameters are introduced:

$$x = \frac{x'}{r_0}, \quad y = \frac{y' Re^{1/2}}{r_0}, \quad r(x) = \frac{r'(x')}{r_0}, \quad t = \frac{U_0 t'}{r_0}$$

$$u = \frac{u'}{U_0}, \quad v = \frac{v' Re^{1/2}}{r_0}, \quad w = \frac{w'}{U_0}, \quad g = \frac{r_0}{U_0^2}g'$$

$$\omega = \frac{r_0\omega'}{U_0}, \quad \theta = \frac{T' - T'_\infty}{T'_w - T'_\infty}, \quad \Lambda = Gr/Re^2. \tag{6}$$

The system of equations (1)–(4) takes the following form:

$$\frac{\partial(ru)}{\partial x} + \frac{\partial(rv)}{\partial y} = 0 \tag{7}$$

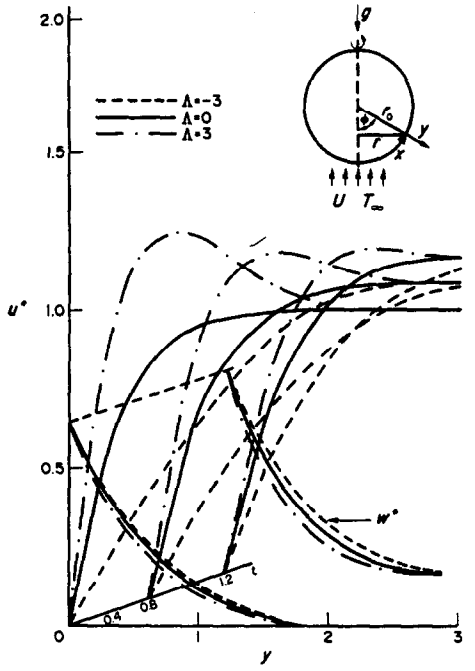

FIG. 1. Profiles of u^* and w^* as functions of y and t for $\omega = \omega_s$, $c = 0$ and $Pr = 0.71$ at $x = 0.6$.

$$\frac{\partial u}{\partial t}+u\frac{\partial u}{\partial x}+v\frac{\partial u}{\partial y}-\frac{w^2}{r}\frac{\partial r}{\partial x}=\frac{\mathrm{d}U}{\mathrm{d}t}+\frac{\partial^2 u}{\partial y^2}+\Lambda\theta r \quad (8)$$

$$\frac{\partial w}{\partial t}+u\frac{\partial w}{\partial x}+v\frac{\partial w}{\partial y}+\frac{wu}{r}\frac{\partial r}{\partial x}=\frac{\partial^2 w}{\partial y^2} \quad (9)$$

$$\frac{\partial \theta}{\partial t}+u\frac{\partial \theta}{\partial x}+v\frac{\partial \theta}{\partial y}=\frac{1}{Pr}\frac{\partial^2 \theta}{\partial y^2}. \quad (10)$$

The boundary conditions for the same dimensionless variables are

$$u = v = w = \theta = 0 \quad \text{at} \quad t \leqslant 0$$

$$u = 0,\ v = c,\ w = r(x)\omega,\ \theta = 1 \ \text{at}\ y = 0,\ t > 0$$

$$u = U,\quad w = 0,\quad \theta = 0 \quad \text{at} \quad y \to \infty,\quad t > 0. \quad (11)$$

Here we consider the uniformly accelerated free stream velocity so that $U = 1.5t \sin x$.

Physical quantities of primary interest are the local Nusselt number Nu and the local friction factor C_f which are defined respectively by

$$Nu = \frac{h_0 r_0}{K},\quad C_f = \frac{2\tau_w}{\rho U_0^2} \quad (12)$$

where the local heat transfer coefficient and the wall shear stress are given respectively by $h_c = q_w/(T'_w - T'_\infty)$ and $\tau_w = \mu(\partial u'/\partial y')_{y'=0}$ where $q_w = -K(\partial T'/\partial y')_{y'=0}$. Using the non-dimensional variables (6) we obtain the relations

$$Nu\, Re^{-1/2} = -\left(\frac{\partial \theta}{\partial y}\right)_{y=0},\quad \tfrac{1}{2}C_f\, Re^{-1/2} = \left(\frac{\partial u}{\partial y}\right)_{y=0}. \quad (13)$$

The numeric solution of parabolic equations (8)–(10) is based on the finite difference approximation, using an extension of the explicit method for one variable in the present case of several variables. Let us describe the method, using an equation of the general form

$$u_t + a_0(x,y,t)u_x + a_1(x,y,t)u_y = au_y^2 + a_3(x,y,t) \quad (14)$$

where u_t represents the partial derivatives of u with respect to the subscript and a is a positive constant. The approximation to $u(nk, ih, jh)$ where k and h represent the steps in time and space, respectively, is denoted by $u^n_{i,j}$. Substituting into equation (14) the approximation $u^n_{t_{i,j}} = (u^{n+1}_{i,j} - u^n_{i,j})/k$ for the derivative with respect to time and using the central difference approximations to first order for the spacial derivatives we obtain

$$u^{n+1}_{i,j} = r_s\left(a + a^n_{1_{i,j}}\frac{h}{2}\right)u^n_{i,j-1} + (1-2ar_s)u^n_{i,j} + r_s\left(a - a^n_{1_{i,j}}\frac{h}{2}\right)u^n_{i,j+1} + a^n_{3,i,j} + O(k^2 + kh^2) \quad (15)$$

where

$$r_s = k/h^2.$$

Extending the method of Richtmyer and Morton [11] for the estimation of the minimum truncation error we have found after detailed calculations that the necessary stability conditions are

$$r_s \leqslant \frac{1}{2a} \quad \text{and} \quad h < \frac{2a}{\|a_1\|} \quad (16)$$

where $\|a_1\| = \max|a_1(x,y,t)|$. The condition for optimal convergence of equation (14) is determined from the requirement to minimize the neglected terms of order k^2 and kh^2, respectively. Rewriting equation (14) as $u_t = au_y^2 + H$ where $H = -(a_1u_y + a_0u_x - a_3)$ this requirement is expressed by

$$L = \frac{k^2}{2}u_t^2 + \frac{kh^2}{6}\delta H - a\frac{kh^2}{12}u_y^4 = \frac{h^4}{4}\left(r_s u_t^2 - \frac{a}{6}u_y^4 + \frac{\delta H}{3}\right) \simeq 0 \quad (17)$$

where $\delta H = a_1u_y^3 - a_0u_x^3$. In the first instant after the motion had been started from rest, the boundary layer is very thin and the viscous term u_y^2 is very large while the convective term H retains its normal values. The term u_y^2 is balanced by the non-steady acceleration u_t together with the pressure gradient (if it exists). Substituting the derivative $u_t^2 = a^2u_y^4 + aH_y^2 + H_t$ into equation (16) we obtain

$$L = \frac{h^4}{2}\left[r_s\left(r_s a - \frac{a}{6}\right)u_y^4 + r_s^2(aH_y^2 + H_t) + r_s\frac{\delta H}{3}\right] \simeq 0. \quad (18)$$

Neglecting the second term which varies like r_s^2 and considering that the contribution of the third term

to the correction is negligible, we observe that the quantity L is minimized for $r_s = 1/(6a)$. This condition for optimal convergence has been verified by extensive numerical calculations.

Applying the above analysis in the system of equations (8)–(10) simultaneously we conclude that the necessary stability conditions are

$$r_s \leqslant \frac{1}{2a_i}(i = u, w, \theta) \quad \text{and} \quad h < \frac{2a_i}{\|u\|} \tag{19}$$

where $\|u\| = \max |u(x, y, t)|$. The coefficients of the second-order partial derivatives a_i take the values $a_u = 1$, $a_w = 1$ and $a_\theta = 1/Pr$. The optimal convergence of the system is achieved when the values of k and h are chosen so that

$$r_s = \varepsilon_1\theta_0(\varepsilon_2 - \varepsilon_1) + \varepsilon_2\theta_0(\varepsilon_1 - \varepsilon_2) \tag{20}$$

where $\varepsilon_1 = \min(1/2a_i)$, $\varepsilon_2 = (a_u^{-1} + a_\theta^{-1})/12$ and θ_0 is the Heaviside step function.

Let us suppose that the solution of equation (14) is subjected to a boundary condition at infinity as it happens with equations (8)–(10). Solving equation (14) and calculating the derivative u_y, we determine the distance y_m at which the boundary condition is imposed, from the continuity condition $u_y(y_m) = 0$ which is satisfied far away from the surface of the sphere.

Although this method introduces a severe restriction on the choice of the time step, it remains a very fast method for the study of physical phenomena within a period of time of the order U_0/r_0. Important quantities require the evaluation of certain derivatives like u_y on the surface of the sphere. These derivatives are evaluated using the Lagrange interpolation formula

$$u^n_{y,i,0} = (-3u^n_{i,0} + 4u^n_{i,1} - u^n_{i,2})/(2h) + O(h^2).$$

RESULTS AND DISCUSSION

The numerical results indicate the velocity and thermal boundary layer growth for gases having a Prandtl number $Pr = 0.71$, under a uniformly accelerated potential flow of the form $U = 1.5t \sin x$. Results of various quantities as functions of x and t are presented for the angular velocities $\omega = \pi/2$ and $3\pi/2$, denoted by ω_s and ω_l, respectively. The buoyancy parameter Λ varies from the pure forced convection $\Lambda = 0$ to the mixed convection values $\Lambda = 3, 10, 50$ for aiding flow and from 0 to -3 for opposing flow. The effects of the suction ($c < 0$) and injection ($c > 0$) are also investigated for the parametric values $c = -0.5$ and 0.5, respectively. The value $c = 0$ corresponds to an impermeable surface.

The variation of the velocity components $u^* = u/U$ and $w^* = w/\omega$ as functions of y and t for $c = 0$, $\omega = \omega_s$ and $\Lambda = -3, 0, 3$ when $x = 0.6$ and 1.2 rad are shown on Figs. 1 and 2, respectively. We observe that for aiding flow, the velocity gradient of u^* at the wall increases as the buoyancy force increases and hence the velocity boundary layer thickness δ_u decreases. Comparing Figs. 1 and 2 we observe that as the angle x increases the velocity u^* decreases rapidly as buoyancy increases for $\Lambda \leqslant 0$, while it increases very slowly as buoyancy increases for $\Lambda > 0$. An overshooting of u is observed beyond the local free stream velocity which increases as the buoyancy increases for aiding flow and decreases gradually as time increases. This is because the buoyancy force inside the boundary layer assists the forced flow. The rotational velocity w^* increases as $|\Lambda|$ increases for $\Lambda < 0$ and decreases as buoyancy increases for $\Lambda > 0$. It seems that w^* becomes less sensitive to buoyancy as ω increases (Fig. 3). When $\omega = \omega_s$ the rotational and forced flow are of comparable magnitude as t varies from 0.8 to 1.2. As ω increases the thickness δ_u decreases while the overshooting of u^* becomes stronger because of the coupling of the buoyancy force to the fast rotation.

The effect of the buoyancy force on u^* when the surface of the sphere is porous subjected to suction $c = -0.5$ or injection $c = 0.5$ is shown on Figs. 4–6. The values $c = -0.5$, 0, 0.5 will be denoted by C_-, C_0 and C_+, respectively. For aiding flow subjected to suction we see a reduction of the overshooting of u^* and a small increase of the thickness δ_u, while in the case of injection δ_u decreases. For opposing flow subjected to suction the velocity u^* increases yielding to a reduction of δ_u, while in the case of injection a significant increase of δ_u is observed. As time increases the velocity profiles are shifted to smaller values in the aiding flow while they are shifted to higher values in the case of opposing flow. The rate of variation of the various profiles as t increases is due to the influence of our free stream velocity. In Fig. 6 similar results are shown for the increased angular velocity $\omega = \omega_l$ when $t = 0.8$ and 1.2. We observe that for $t = 0.8$, in

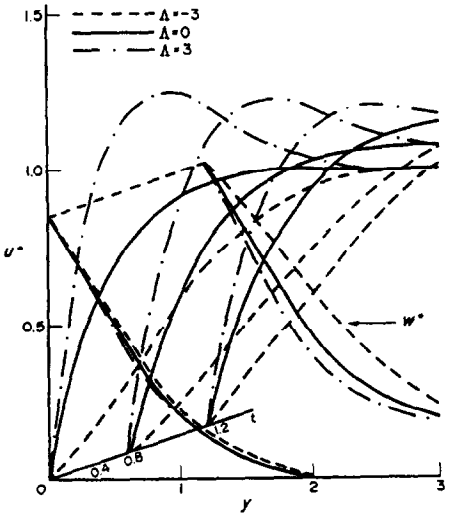

FIG. 2. Profiles of u^* and w^* as functions of y and t for $\omega = \omega_s$, $c = 0$ and $Pr = 0.71$ at $x = 1.2$.

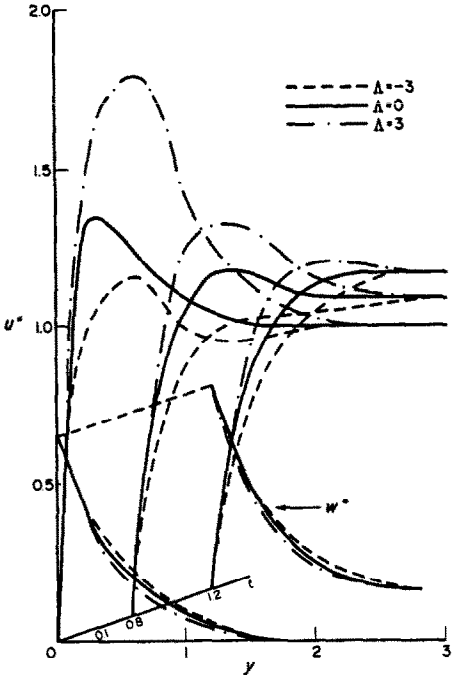

FIG. 3. Profiles of u^* and w^* as functions of y and t for $\omega = \omega_i$, $c = 0$ and $Pr = 0.71$ at $x = 0.6$.

opposing flow, the injection yields to a higher velocity profile than the corresponding one in the case of suction. This is due to the fact that when $\omega \gg U$ the rotational forces cause the decrease of the values of the vertical velocity v. This effect which is much stronger in the case of injection results in the increase of u^*. Hence for $\Lambda < 0$ and $\omega \gg U$ the thickness δ_u takes lower values imposing injection than imposing suction. As U increases with time this behaviour is reversed. The low profile of u^* in the opposing flow is due to the effect of the low rate of thermal flow from the free stream to the sphere.

The variation of the temperature $\theta(y, t)$ for various

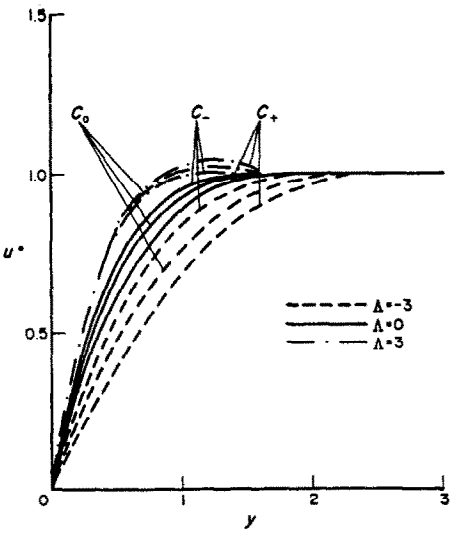

FIG. 5. Profiles of u^* for $\omega = \omega_s$, $Pr = 0.71$, $x = 0.6$ and $t = 1.2$.

values of Λ and c when $x = 0.6$ and $\omega = \omega_s$ are shown on Fig. 7, while similar results are presented in Table 1 for $x = 1.2$ and $t = 0.8$ when $\omega = \omega_s$, ω_i. Figure 7 shows that as the buoyancy increases the temperature decreases in the aiding flow while it increases in the opposing flow. The effect of buoyancy forces of small magnitude on the temperature is not significant. As the suction increases the temperature decreases while in the case of injection this behaviour is reversed. The temperature increases with the angle x. The coupling of suction with increasing aiding flow reduces further the thermal boundary layer thickness δ_θ while the coupling of injection with increasing opposing flow increases further the thickness δ_θ. The increase of the rotation reduces the temperature profile and increases its steepness except in the case $c = -0.5$, $\Lambda = -3$ (Table 1). The free stream causes a small increase of the temperature as time varies from 0 to the vicinity

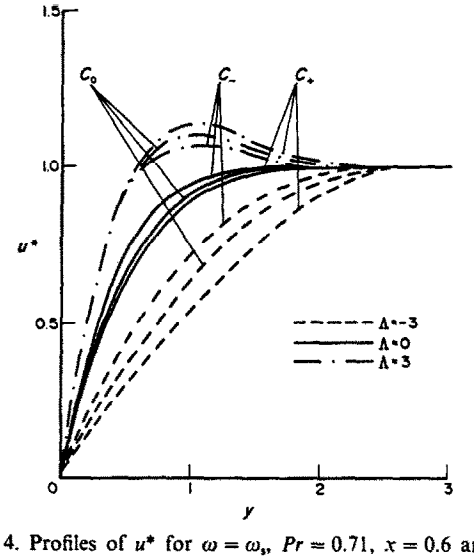

FIG. 4. Profiles of u^* for $\omega = \omega_s$, $Pr = 0.71$, $x = 0.6$ and $t = 0.8$.

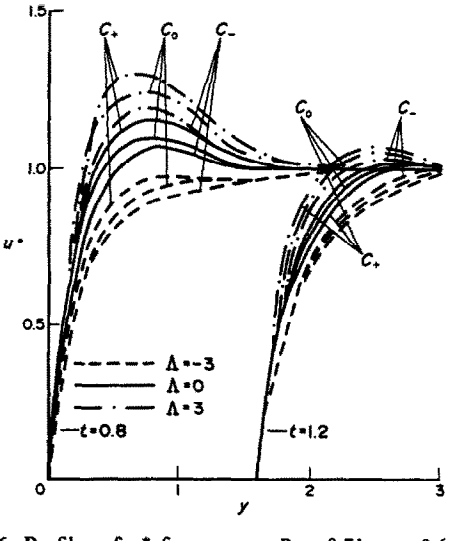

FIG. 6. Profiles of u^* for $\omega = \omega_i$, $Pr = 0.71$, $x = 0.6$ and $t = 0.8$, 1.2.

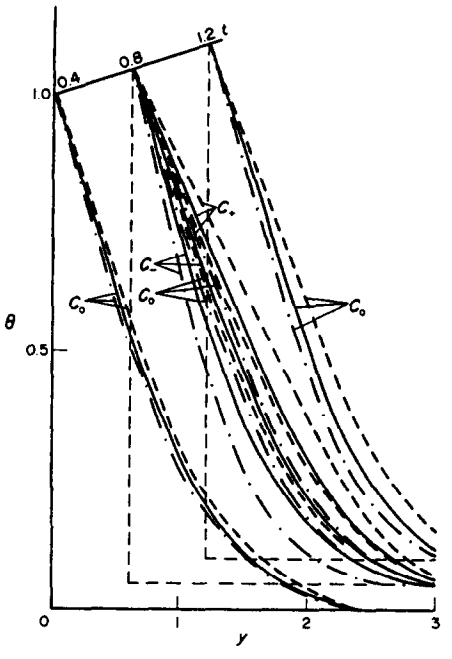

FIG. 7. Profiles of temperature θ as functions of y and t for $\omega = \omega_s$, $Pr = 0.71$ and $x = 0.6$.

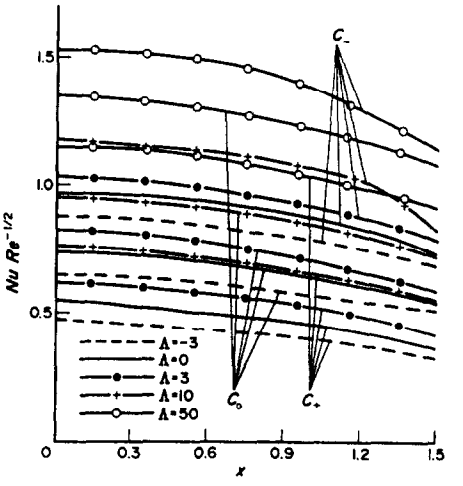

FIG. 8. Angular distribution of the local Nusselt number for $\omega = \omega_s$, $Pr = 0.71$ and $t = 0.8$.

of 0.7 (Fig. 7) for $0 \leqslant x \leqslant 1.5$. As time t and U increase further the temperature decreases slowly for positive or negative Λ and angles in the range $0 \leqslant x \leqslant 0.78$. For $x > 0.78$ the temperature continues to decrease slowly for $\Lambda \geqslant 0$ while it increases for $\Lambda < 0$. This is due to the very small values of the velocity u^* when $\Lambda < 0$ and $t > 0.7$ (Figs. 1 and 2). Increasing ω the situation is reversed and the temperature decreases again as $x > 0.78$ and $\Lambda < 0$ for $t > 0.7$ (Table 1, see $c = 0$, $\Lambda = -3$ at $t = 1.2$).

The angular distribution of the local Nusselt number in terms of $Nu\ Re^{-1/2}$ for buoyancy parameters $-3 \leqslant \Lambda \leqslant 50$ and $c = -0.5, 0, 0.5$ are shown on Figs. 8 and 9 for $\omega = \omega_s$ at $t = 0.8$, 1.2 and on Fig. 10 for $\omega = \omega_l$ at $t = 0.8$. The local surface heat transfer rate increases as the buoyancy force increases for aiding flow, while an opposite trend is observed for opposing flow. The Nusselt number decreases as the angle x increases from the stagnation point. Imposing suction the number $Nu\ Re^{-1/2}$ increases while imposing injection it decreases. Figure 9 indicates that as the buoyancy forces vary from moderate to small values the local Nusselt number depends strongly on the variation of the local free stream velocity and increases as time increases. This effect becomes more pronounced in the opposing flow as x increases. Increasing ω the Nusselt number is shifted to higher values for small and moderate buoyancy forces while it becomes less sensitive as buoyancy increases to large values.

The relative changes in the local Nusselt number Nu/Nu_0, where Nu_0 is the Nusselt number at the stagnation point are shown on Fig. 11 for various values of Λ, c and ω at $t = 0.8$. For small rotations the angular variation of Nu/Nu_0 is greater in the case of $\Lambda = 0$ and 3 than the corresponding one for $\Lambda = -3$. Imposing injection this effect becomes much more pronounced in contrast to the case of suction. As ω

Table 1. Effect of buoyancy Λ and rotation ω on the temperature θ when $c = -0.5, 0, 0.5$ at $t = 0.8$. The case for $\Lambda = -3$ and $c = 0$ at $t = 1.2$ is also shown

	$t = 0.8, \Lambda = -3$			$t = 0.8, \Lambda = 0$			$t = 0.8, \Lambda = 3$			$t = 1.2, \Lambda = -3$
y	$c = -0.5$	$c = 0$	$c = 0.5$	$c = -0.5$	$c = 0$	$c = 0.5$	$c = -0.5$	$c = 0$	$c = 0.5$	$c = 0$
					ω_s					
0.0	1	1	1	1	1	1	1	1	1	1
0.3	0.7852	0.8370	0.8816	0.7679	0.8692	0.8645	0.7505	0.8043	0.8456	0.8557
0.6	0.5959	0.6788	0.7556	0.5635	0.6429	0.7187	0.5318	0.6062	0.6790	0.7119
0.9	0.4330	0.5293	0.6254	0.3912	0.4786	0.5691	0.3521	0.4296	0.5115	0.5693
1.2	0.2974	0.3919	0.4945	0.2538	0.3340	0.4239	0.2159	0.2819	0.3572	0.4307
1.5	0.1889	0.2688	0.3658	0.1511	0.2142	0.2909	0.1207	0.1685	0.2270	0.3006
					ω_l					
0.0	1	1	1	1	1	1	1	1	1	1
0.3	0.7861	0.8362	0.8782	0.7596	0.8065	0.8475	0.7384	0.7833	0.8239	0.7955
0.6	0.5967	0.6759	0.7467	0.5473	0.6167	0.6814	0.5098	0.5730	0.6340	0.5879
0.9	0.4331	0.5243	0.6108	0.3702	0.4421	0.5129	0.3255	0.3862	0.4481	0.3860
1.2	0.2969	0.3859	0.4763	0.2323	0.2934	0.3562	0.1906	0.2374	0.2869	0.2043
1.5	0.1883	0.2642	0.3475	0.1328	0.1766	0.2228	0.1010	0.1310	0.1631	0.0595

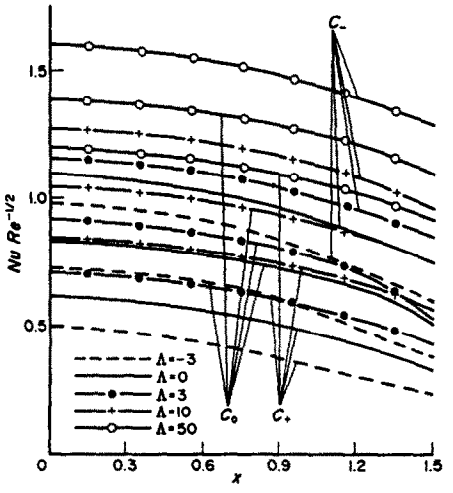

FIG. 9. Angular distribution of the local Nusselt number for $\omega = \omega_s$, $Pr = 0.71$ and $t = 1.2$.

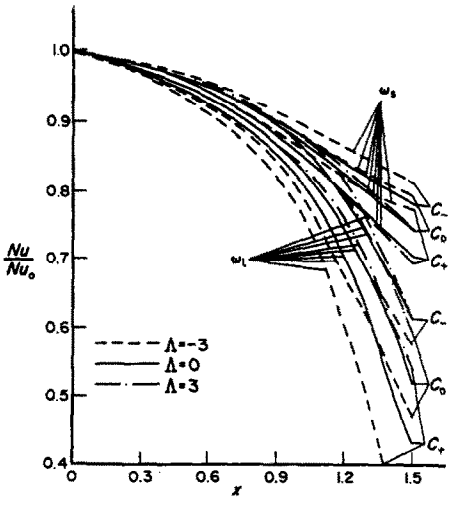

FIG. 11. Relative angular distribution of the local Nusselt number for $Pr = 0.71$ and $t = 0.8$.

increases to much higher values the picture changes completely. The angular variation of Nu/Nu_0 is greater as buoyancy decreases for aiding flow and increases for opposing flow. The angular change of the local Nusselt number increases as injection increases and decreases as suction increases.

A direct measure of the significance of the buoyancy force is given by the ratio Nu_0/Nu_{0f}, where Nu_{0f} is the local Nusselt number for pure forced convection ($\Lambda = 0$). The variations of these ratios for various values of the parameters Λ and c are shown in Fig. 12 for $\omega = \omega_s$, ω_l and $t = 0.8$. We define as the threshold of significance of the buoyancy the departure from the pure forced convection by 5%. Then the limits of significance of the buoyancy in the cases of suction, injection and impermeable wall for $\omega = \omega_s$, ω_l at $t = 0.8$ are shown in Table 2. At $t = 1.2$ the results obtained are very close to those of Table 2. The results indicate that when injection increases the thresholds of significance of buoyancy forces decrease in the opposing and aiding flows while for increasing suction these thresholds increase. The opposing flow is more sensitive to the buoyancy forces than the aiding flow. The increase of the rotation causes the increase of the corresponding thresholds.

The effects of buoyancy forces, of suction, injection and rotation on the angular distribution of the local wall stress $\tau = 0.5 C_f Re^{-1/2}$ are shown for various parametric values in Fig. 13 and Table 3. The quantity τ increases as the buoyancy force, the rotation and the suction increase, while it decreases as injection increases. However, in comparison with buoyancy suction, injection and rotation have a more pronounced effect. The decrease of τ and Λ decreases and injection increases yields a shift of the separation point of the flow toward the stagnation point. On the contrary the increase of τ results in a delay in the separation of the flow. For very large buoyancy values according to Suwono [3] the separation occurs not due to the collision of the flow but to the vanishing of the local stream stress at the wall. Comparing our results for τ, with those obtained using the time independent potential velocity $u(x, \infty, t) = U_e = 1.5 \sin x$ as a boundary condition, we see that the time-dependent potential velocity $U = U_e t$ moves the separation point towards the equator. For sufficiently large values of U the separation will be caused by the vanishing of the local wall shear stress at the surface of

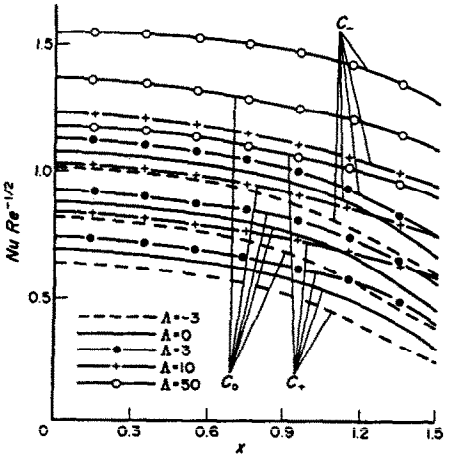

FIG. 10. Angular distribution of the local Nusselt number of $\omega = \omega_l$, $Pr = 0.71$ and $t = 0.8$.

Table 2. Thresholds of significance of buoyancy forces in the opposing and aiding flow when $c = -0.5, 0, 0.5$ at $t = 0.8$

$t = 0.8$	ω_s		ω_l	
	$\Lambda < 0$	$\Lambda > 0$	$\Lambda < 0$	$\Lambda > 0$
C_-	−1.85	1.90	−3.00	3.30
C_0	−1.40	1.45	−2.50	2.85
C_+	−1.05	1.10	−2.15	2.17

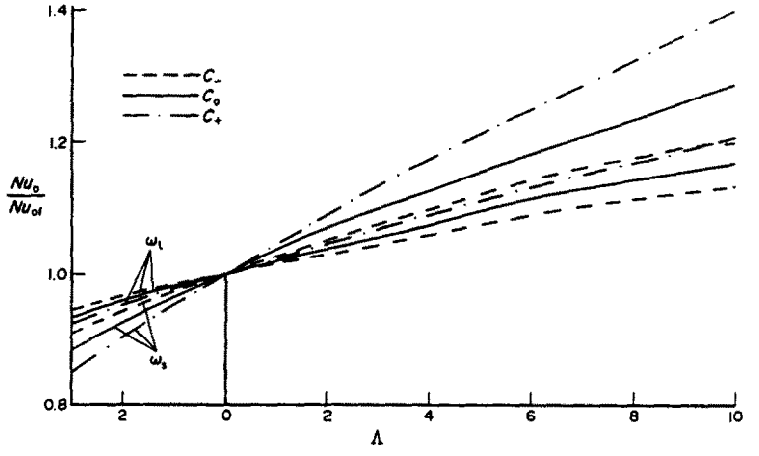

FIG. 12. Effects of buoyancy on the heat transfer at the stagnation point for $Pr = 0.71$ and $t = 0.8$.

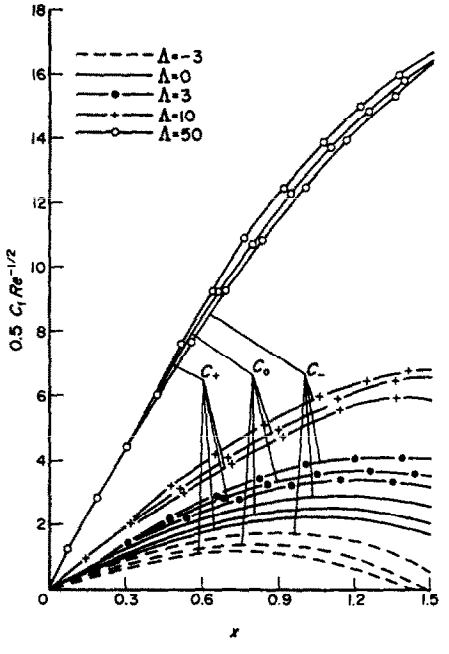

FIG. 13. Angular distribution of the local friction factor for $\omega = \omega_3$, $Pr = 0.71$ at $t = 1.2$.

the sphere and not by the collision of the flow at the surface.

At this point it is interesting to compare results obtained with our method with those obtained from other experimental and numerical works. The experimental results presented by Yuge for mixed convection at very low Reynolds and Grashof numbers ($Re = 1.8$–55, $Gr = 0.125$–230) indicated the average Nusselt numbers $\overline{Nu}\ Re^{-1/2}$ of 0.706 and 1.643, respectively, for $\Lambda = 1$ and 50. Chen and Mucoglu in their numerical study of the steady state of a non-rotating sphere using the boundary layer approximation, predicted local Nusselt numbers $Nu\ Re^{-1/2}$ ranging from 0.842 to 0.486 for $\Lambda = 1$, from 1.312 to 1.071 for $\Lambda = 50$ as x increases from 0 to 1.4 and $Nu\ Re^{-1/2} = 0.8149$ at $\Lambda = 0$. Rajasekaran and Palekar in a similar numerical study for the mixed convection about a rotating sphere predicted the number $Nu\ Re^{-1/2} = 0.838$ at $\Lambda = 0$. Solving now our problem, using the time independent boundary condition $u(x, \infty, t) = U_e$ instead of $u(x, \infty, t) = U_e t$ (see equation (11)), our method reaches the limit of steady state at $t = 2$ when $c = 0$. Our results for the case of a non-rotating sphere, predicted a local Nusselt

Table 3. Effect of buoyancy Λ and rotation ω on the local friction factor $0.5 C_f\ Re^{-1/2}$ when $c = -0.5$, 0, 0.5 at $t = 0.8$. The case for $\Lambda = 0$, $c = 0$ for $U = U_e$ is also shown

	$\Lambda = -3$			$\Lambda = 0$			$\Lambda = 3$			U_e, $\Lambda = 0$
X	$c = -0.5$	$c = 0$	$c = 0.5$	$c = -0.5$	$c = 0$	$c = 0.5$	$c = -0.5$	$c = 0$	$c = 0.5$	$c = 0$
					ω_3					
0.0	0.0001	0.0001	0.0001	0.0002	0.0002	0.0002	0.0003	0.0003	0.0003	0.0003
0.3	0.4387	0.3616	0.3037	0.7974	0.7334	0.6754	1.1086	1.0582	1.0052	0.7893
0.6	0.7717	0.6196	0.5054	1.4792	1.3529	1.2383	2.0938	1.9937	1.8880	1.4386
0.9	0.8806	0.6592	0.4941	1.9278	1.7429	1.5752	2.8408	2.6922	2.5346	1.7834
1.2	0.7269	0.4462	0.2393	2.0753	1.8364	1.6210	3.2697	3.0739	2.8648	1.7373
1.5	0.3509	0.0320	−0.1983	1.9014	1.6170	1.3644	3.3306	3.0883	2.8306	1.2694
					ω_1					
0.0	0.0004	0.0004	0.0004	0.0005	0.0005	0.0005	0.0006	0.0006	0.0006	0.0005
0.3	1.1992	1.2420	1.2807	1.4300	1.4688	1.5012	1.6487	1.6869	1.7164	1.4374
0.6	2.1628	2.2349	2.2987	2.6330	2.6968	2.7477	3.0754	3.1381	3.1829	2.6215
0.9	2.6744	2.7508	2.8109	3.4071	3.4654	3.5008	4.0886	4.1455	4.1728	3.3040
1.2	2.4486	2.5073	2.5564	3.5508	3.5794	3.5744	4.4968	4.5031	4.4633	3.2314
1.5	0.7623	0.5120	0.3345	2.5624	2.4084	2.2418	4.0831	3.9943	3.8422	2.0360

number $Nu\,Re^{-1/2}$ ranging from 0.848 to 0.54 for $\Lambda = 1$ and from 1.33 to 1.07 for $\Lambda = 50$ as x increases from 0 to 1.4, and $Nu\,Re^{-1/2} = 0.825$ for $\Lambda = 0$. Imposing rotation when $c = 0$ and $\Lambda = 0$ the number $Nu\,Re^{-1/2}$ ranges from 0.84 to 0.49 at $\omega = \omega_s$ and from 0.95 to 0.53 at $\omega = \omega_l$ as x varies from 0 to 1.4. The agreement between the theoretical and experimental results is fair for $\Lambda = 1$ and very poor for $\Lambda = 50$ because our results are based on the boundary-layer approximation which is valid in the case of large Reynolds and Grashof numbers.

REFERENCES

1. B. T. Chao and R. Greif, Laminar forced convection over rotating bodies, *ASME J. Heat Transfer* **96**, 463–466 (1974).
2. M. H. Lee, D. R. Jeng and K. J. De Witt, Laminar boundary layer transfer over rotating bodies in forced flow, *ASME J. Heat Transfer* **100**, 496–502 (1978).
3. A. Suwono, Buoyancy effects on flow and heat transfer on rotating axisymmetric round-nosed bodies, *Int. J. Heat Mass Transfer* **23**, 819–831 (1980).
4. T. S. Chen and A. Mucoglu, Analysis of mixed forced and free convection about a sphere, *Int. J. Heat Mass Transfer* **20**, 867–875 (1977).
5. R. Rajasekaran and M. G. Palekar, Mixed convection about a rotating sphere, *ASME J. Heat Mass Transfer* **28**, 959–968 (1985).
6. C. A. Hieber and B. Gebhart, Mixed convection from a sphere at small Reynolds and Grashof numbers, *J. Fluid Mech.* **38**, 137–159 (1969).
7. T. Yuge, Experiments on heat transfer from spheres including combined natural and forced convection, *J. Heat Transfer* **82C**, 214–220 (1960).
8. L. S. Klyachko, Heat transfer between gas and a spherical surface with the combined action of free and forced convection, *J. Heat Transfer* **85C**, 355–357 (1963).
9. G. C. Pande and P. Hatzikonstantinou, Numerical treatment of hydromagnetic thermal boundary-layer flow of an infinite porous limiting surface, *Astrophys. Space Sci.* **107**, 313–322 (1984).
10. P. Hatzikonstantinou, Unsteady hydromagnetic thermal flow past a cylinder in presence of magnetic field, *ZAMM* **66**, 57–60 (1986).
11. R. D. Richtmyer and K. W. Morton, *Difference Methods for Initial-value Problems*, p. 16. Interscience, New York (1967).

CONVECTION MIXTE VARIABLE POUR UNE SPHERE POREUSE TOURNANTE

Résumé—On présente l'étude des caractéristiques de l'écoulement et du transfert de chaleur lors de la croissance de la couche limite autour d'une sphère en rotation soumise à une accélération uniforme. Des résultats sont présentés pour des gaz à nombre de Prandtl de 0,71 et différentes valeurs de flottement et de rotation, lorsque la surface est solide, ou poreuse soumise à succion ou injection. On applique une méthode numérique pour laquelle on détermine les conditions de stabilité et de convergence optimale. On trouve que le nombre de Nusselt local et le coefficient de frottement local augmentent quand augmente le flottement pour un écoulement avec succion et décroît lorsque le flottement augmente mais avec injection. Le seuil de signification des forces de flottement s'abaisse quand l'injection augmente et monte quand la succion croît.

UNSTETIGE MISCHKONVEKTION AN EINER PORÖSEN ROTIERENDEN KUGEL

Zusammenfassung—Strömung und Wärmetransport bei instationärem Grenzschichtwachstum an einer rotierenden Kugel in einer erzwungenen Strömung werden untersucht, wobei die Strömung durch einen gleichförmig beschleunigten Freistrahl hervorgerufen wird. Es werden Ergebnisse für Gase bei einer Prandtl-Zahl von 0,71 und für verschiedene Auftriebs- und Rotationswerte vorgestellt, wobei die Oberfläche fest oder porös sein kann und letztere einem Absaugen oder Einblasen unterliegt. Es wird ein numerisches Verfahren angewandt, für das die Stabilitätsbedingungen und die optimale Konvergenz bestimmt werden. Die örtliche Nusselt-Zahl und der örtliche Reibungsfaktor nehmen mit zunehmendem Auftrieb bei zusätzlicher Strömung durch Absaugen zu, während sie mit zunehmendem Auftrieb und Einblasen abnehmen. Die Schwelle für die Bedeutung der Auftriebskräfte nimmt mit zunehmendem Einblasen ab und mit zunehmendem Absaugen zu.

НЕСТАЦИОНАРНАЯ СМЕШАННАЯ КОНВЕКЦИЯ ОКОЛО ПОРИСТОЙ ВРАЩАЮЩЕЙСЯ СФЕРЫ

Аннотация—Исследуются характеристики течения и теплопереноса в растущем нестационарном пограничном слое около вращающейся сферы в вынужденном потоке, обусловленном постоянно ускоренным свободным течением. Представлены результаты для газов с $Pr = 0{,}71$ и различными значениями подъемной силы и числа вращения, полученными для случаев твердой или пористой поверхности при наличии на ней всасывания или вдува. Используется численный метод, для которого определены условия устойчивости и оптимальной сходимости. Найдено, что локальное число Нуссельта и локальный коэффициент трения увеличиваются с ростом подъемной силы в случае спутного потока при наличии всасывания и уменьшаются с ростом подъемной силы при вдуве. Порог эффективности подъемных сил снижается с увеличением вдува и возрастает с усилением всасывания.